Bone 187 (2024) 117213

Contents lists available at ScienceDirect

Bone

journal homepage: www.elsevier.com/locate/bone

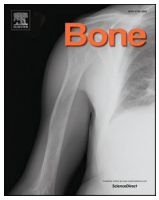

Full Length Article

Enhancing the biological integration of massive bone allografts: A porcine preclinical in vivo pilot-study

Robin Evrard [a,b,c,g,*], Julie Manon [a,c,d,g], Louis Maistriaux [b,d], Lies Fievé [d], Tom Darius [b,e], Olivier Cornu [a,c,g], Benoit Lengelé [d,f,1], Thomas Schubert [a,c,g,1]

[a] Institut de Recherche Expérimentale et Clinique, Neuro Musculo-Skeletal Lab, Université Catholique de Louvain, Avenue E. Mounier, 52-B1.52.04 – 1200, Bruxelles, Belgium
[b] Institut de Recherche Expérimentale et Clinique, Pôle Chirurgie Expérimentale et Transplantation, Université Catholique de Louvain, Avenue E. Mounier, 52-B1.52.04 – 1200, Bruxelles, Belgium
[c] Service de Chirurgie Orthopédique et Traumatologique, Cliniques Universitaires Saint-Luc, Avenue Hippocrate 10-1200, Bruxelles, Belgium
[d] Institut de Recherche Expérimentale et Clinique, Pôle Morphologie, Université Catholique de Louvain, Avenue E. Mounier, 52-B1.52.04 – 1200, Bruxelles, Belgium
[e] Département de Chirurgie, Chirurgie abdominale et unité de transplantation, Cliniques Universitaires Saint-Luc, Avenue Hippocrate 10-1200, Bruxelles, Belgium
[f] Service de Chirurgie Plastique, Reconstructrice et Esthétique, Cliniques Universitaires Saint-Luc, Avenue Hippocrate 10-1200, Bruxelles, Belgium
[g] Unité de Thérapie Tissulaire et Cellulaire de l'Appareil Locomoteur, Cliniques Universitaires Saint-Luc, Avenue Hippocrate 10-1200, Bruxelles, Belgium

ARTICLE INFO

Keywords:
Massive bone allograft
Perfusion-decellularization
In vivo osseointegration
Bone remodeling
Histology & immunohistochemistry

ABSTRACT

Critical bone loss can have several origins: infections, tumors or trauma. Therefore, massive bone allograft can be a solution for limb salvage. Such a biological reconstruction should have the ideal biomechanical qualities. However, their complication rate remains too high. Perfusion-decellularization of massive allografts could promote the vitality of these grafts, thereby improving their integration and bone remodeling.

Three perfusion-decellularized massive bone allografts were compared to 3 fresh frozen massive bone allografts in a preclinical in vivo porcine study using an orthopedic surgery model. Three pigs each underwent a critical diaphyseal femoral defects followed by an allogeneic intercalary femoral graft on their both femurs (one decellularized and one conventional fresh frozen as "native") to reconstruct the defect. Clinical imaging was performed over 3 months of follow-up. The grafts were then explanted and examined by non-decalcified histology, fluoroscopic microscopy and immunohistochemistry.

Bone consolidation was achieved in both groups at the same time. However, the volume of bone callus appeared to be greater in the decellularized group. Histology demonstrated a superior bone remodeling in the decellularized group, with a higher number of osteoclasts ($p < 0.001$) and larger areas of osteoid matrix and newly formed bone as compared to the "native" group. Immunohistochemistry showed a superior vitality and remodeling in both the cortical and medullary cavities for osteocalcin ($p < 0.001$), Ki67 ($p < 0.001$), CD3 ($p < 0.001$) and α-SMA ($p < 0.001$) as compared the "native" group. Three months after implantation, the decellularized grafts were proven to be biologically more active compared to native grafts. Fluoroscopic microscopy revealed more ossification fronts in the depth of the decellularized grafts ($p = 0.021$).

This pilot study provides the first in vivo demonstration on the enhanced biological capacities of massive bone allograft decellularized by perfusion as compared to conventional massive bone allografts.

1. Introduction

Massive bone defects remain a major surgical challenge in complex limb reconstructions. Indications may vary (e.g., oncological, traumatic, septic, non-unions, malformations) and require multidisciplinary care and high demanding case-by-case management [1]. Since the advent of limb salvage surgery, many different reconstructive techniques have been developed.

* Corresponding author at: Institut de Recherche Expérimentale et Clinique, Neuro Musculo-Skeletal Lab, Université Catholique de Louvain, Avenue E. Mounier, 52-B1.52.04 – 1200, Bruxelles, Belgium.
E-mail address: robin.evrard@uclouvain.be (R. Evrard).
[1] Both authors have equally contributed to this work.

https://doi.org/10.1016/j.bone.2024.117213
Received 18 May 2024; Received in revised form 2 July 2024; Accepted 23 July 2024
Available online 29 July 2024

Critical bone defects can be reconstructed either with metallic implants, grafting techniques -autografts, allografts or xenografts - specific surgical techniques - Masquelet's technique or distraction osteogenesis - or finally with bone substitutes such as ceramic, bioactive glass and3D-printed calcium-phosphate implants. Metallic implants, in addition to having a high infection rate, are quite expensive and the manufacturing time for custom-made is relatively long [2,3]. Autografts show the best results but remain available in limited quantities and adaptability. They are often not sufficient for large bone loss and are burdened by complications at the donor-site [4,5]. Non-metallic bone substitutes are currently being studied extensively. However, their biological efficacy remains questionable and they have the same disadvantages as mentioned above for metallic implants [5]. Because of higher complication rate and immunogenic issues, xenografts in orthopedics are slowly starting to fade away in the current worldwide practice [6,7]. Masquelet's technique or distraction osteogenesis require either two-stage surgery or a very long treatment period and are not devoid of complications [8,9]. Massive bone allografts, on the other hand, are much cheaper and can be readily available through local bone banks [10]. However, they have a too high complication rate in the short-, medium- and long-term follow-up [11–13] to make them a gold standard in limb salvage surgery. As Delloye et al. exposed, "*one way to minimize the allograft complications is to improve its incorporation*" [13]. This work focuses on improvements that can be brought to the biological integration of massive bone allografts.

Our research hypothesis is based on the fact that conventional massive bone allografts are neither processed nor decellularized before implantation. We believe that the inherent complications in massive allografts surgeries are mainly due to the residual immunogenic load of the grafted tissue [14,15]. Removing this immunogenicity should therefore improve the creeping substitution within the grafts [13]. The latest research in the tissue engineering field demonstrates the feasibility of whole-organ decellularization via the arterial network [16–19]. These advances allow to acquire biocompatible and non-immunogenic tissue models for an almost-complete cellular recolonization [16,20]. Many studies are still underway in vitro but some are very encouraging for in vivo application [21–23].

Our team has set up a protocol for decellularization by perfusion of porcine long bones (humeri and femurs). This protocol, described in a previous study [19], allowed us to obtain completely cleaned and decellularized massive bone allografts. This process exploits the nutrient artery as the main perfusion path for decellularization. The quality of decellularization and loss of immunogenicity acquired with this NaOH-based protocol was shown to be better on bones compared to other protocols more commonly used in the literature (SDS, Triton-X or DNAse) [24–26].

This study is the first pre-clinical in vivo application of our perfusion-decellularized massive bone allograft model. The animal model chosen was the pig. This large animal model is a well-known pre-clinical model for human translation, especially in the field of transplantation surgery. Moreover, the bone structure of the pig is highly comparable to the human bone structure [27]. Finally, this animal is easy to manage as a surgical experimental model [28–31].

This animal study is a pilot study which tends to prove the superior osseointegration of perfusion-decellularized massive bone allografts compared to conventional fresh-frozen ones. Therefore, our initial theoretical hypothesis about residual immunogenic tissue inside the graft is tested. More specifically, we will evaluate the quality of osseointegration of our allografts through several methods: by osteoclasts histomorphometry, qualitatively assessing histological mineralization of consolidation tissue, quantitatively evaluating immunohistochemistry targeting relevant osseointegration markers, using fluorescent microscopy of histological sections to highlight active ossification fronts in the grafts, and performing conventional clinical imaging to assess the kinetics of bone callus growth.

2. Material and methods

Three Aachen Minipigs were used in these experiments.

All experiments were approved by the local ethics committee of UCLouvain (Brussels, Belgium) and carried out in accordance with the Belgian (Royal Decree, September 2004) and European legislations (Directive-2010-63 UE) concerning animals used in experiments (ethical agreements: 2020/UCL/MD/027 for harvested bones and 2021/UCL/MD/062 for surgical experiments).

2.1. Allografts harvesting

Six paired femurs were taken from three 50 kg donor female Belgian-Landrace pigs of two years old (RA-SE Genetics®, Lokeren, Belgium). Each femur was harvested and dissected non-sterile. Their nutrient artery was isolated and cannulated. A complete flushing of the bone vasculature was performed by injecting warm heparinized physiological fluid (25.000 I.U./L) through this vascular network until transparent venous return was observed. The femurs were then labelled by pair and stored at −80 °C.

2.2. Decellularization and imaging

From each pair of femurs, one of the two were randomly allocated to the "decellularized" group. The other was allocated to the "native" group. The latter acted as a conventional massive bone allograft as used nowadays in clinics. Bones of decellularized group underwent the decellularization protocol by perfusion of their nutrient artery according to the previously described protocol [19]. This protocol consists of a precise sequence of solvents perfusion through each bone, the solvents used are pure acetone (48-h perfusion), pure sodium hydroxide (1-h perfusion) and 7,5 % hydrogen peroxide (16-h perfusion). Each sequence is followed by a phosphate-buffered saline rinsing phase of minimum 24 h each. The femurs were perfused while being immerged into the corresponding solvent. All experiments were conducted under room temperature and atmospheric pressure. The femurs were then stored at −80 °C and scanned to ensure best fitting between the graft and the surgical critical-sized bone defect using a clinical CT scanner with 128 detectors (Siemens Definition AS, Erlangen, Germany).

2.3. Allograft cutting and sterilization

The massive bone allograft corresponded to an intercalary femoral diaphyseal segment of 2.5 cm length, corresponding to a critical-sized bone defect [30,32]. Based on the previous CT-scan acquisitions, Patient Specific Instrument (PSI) were created (3D-Side®, Louvain-la-Neuve) to precisely cut the allograft and the recipient bone (Fig. 1A). A condylar marker was used to control the height of the cut and parallel flat beds ensured the orientation of the oscillating saw blade. The PSI was stabilized by Kirschner wires (Fig. 1B-C). The grafts (Fig. 1D) were labelled and stored separately. They were then sent to irradiation for sterilization (30,000 Grey). Cortical remnants from the femurs were used to perform histological evaluations on native and decellularized grafts prior implantation.

2.4. Large animal model

Three 50 kg recipient female Aachen Minipigs of two years old were used (Carfil Quality®, Oud-Turnhout, Belgium). After 10 days of acclimatization period, each pig was anesthetized by an intra-muscular (IM) injection of 6 mg/kg of Zoletil 100® (Virbac, Carros, France) and 2 mg/kg of Rompun® (Bayer, Leverkusen, Deutschland). A CT-scan of the pelvis and lower limbs was acquired to accurately size their femurs and allocate the previously scanned allografts to match their nearest similar dimensions.

The same surgical team performed all surgeries, as did the position

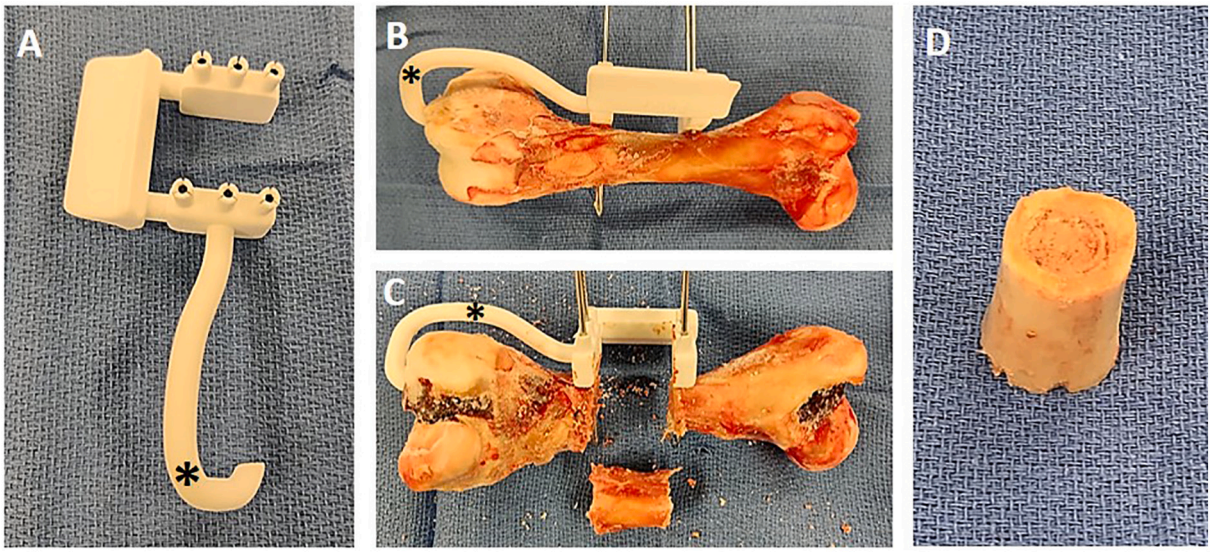

Fig. 1. Images from a control allograft cutting. A: Specific cutting guide (PSI). B: Fixation of the PSI with four K-wires. The right position is achieved thanks to the condylar marker. C: Raw cut of the allograft. D: Cleaned allograft prior implantation.

occupied by each member of the team (lead surgeon, assistant surgeon, instrumentalist, anesthetist). All surgeries were standardized and the equipment used throughout the surgical procedures was also strictly identical from one surgery to the next. The instrument set, power tools, plates and screws were all supplied by Depuy Synthes Vet, Johnson&Johnson, Warsam, Indiana, USA (Small Fragment LCP Plate Set #103.516 & Small Fragment Instrument Set #103.503). The precise description of the surgical procedure is available as supplementary data.

Briefly, recipient pigs were anesthetized using the same IM injection of Zoletil and Rompun and gaseous anesthesia was maintained with Isoflurane (Forene®, AbbVie, Wavre, Belgium) (0–1.5 %) and oxygen. Antibioprophylaxis was achieved with intravenous (IV) Cephazolin as in a standard clinical setup. The pigs were installed on their side, disinfected with iodine and draped to perform a lateral approach of the femur. As described by Schubert et al., the minimum dimension for creating a critical bone defect is 1.5 times the diameter of the concerned diaphysis [30]. In our model, the critical bone defect is 2.5 cm long. The allograft is also 2.5 cm long to ensure the best possible match between the defect and the graft. These dimensions were maintained to the nearest millimeter at all stages, thanks to the use of patient-specific instruments (PSI) for both the graft and the defect. This defect size is also the maximum for effective osteosynthesis. If the defect were any larger,

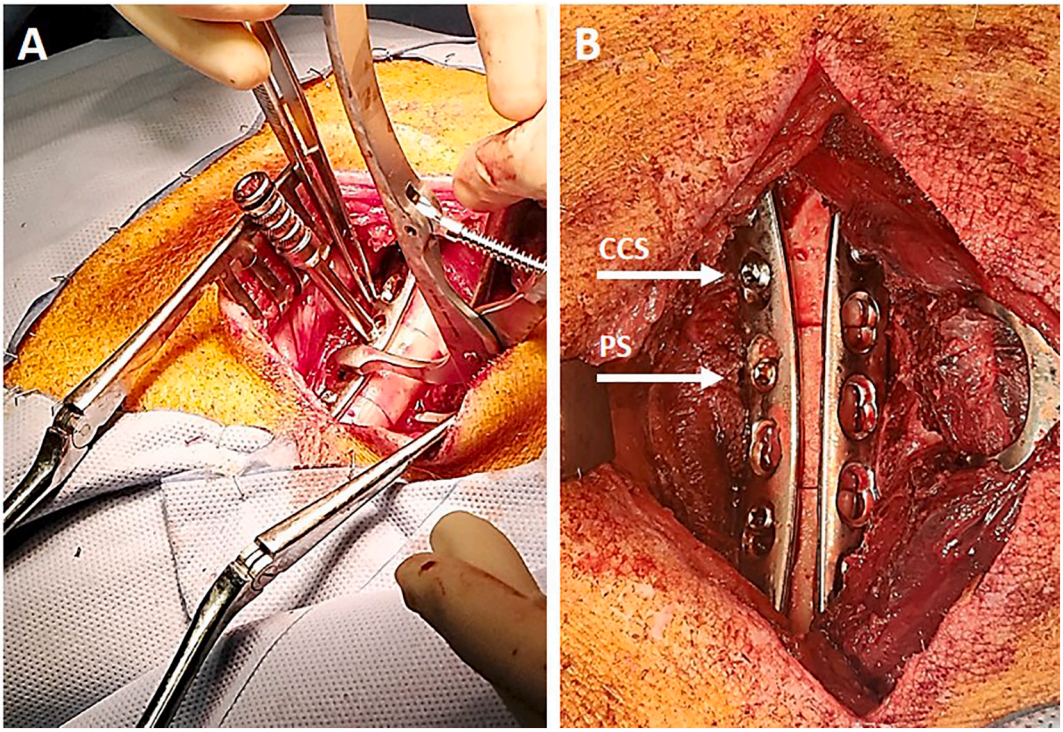

Fig. 2. Grafting and osteosynthesis. A: Allograft temporarily stabilized with forceps against the first plate. Hole of the allograft positional screw is performed. B: Final osteosynthesis with two orthogonal plates. The allograft positional screw (LCP) is highlighted with the white arrow. The compression cortical screw is highlighted with the black arrow.

stabilization would have been compromised with less than three proximal and three distal screws. The allograft was secured in place by two orthogonal 3.5 mm Locking Compression Plates (Fig. 2).

Hydration, analgesia and antibiotic administration was provided through an ear perfusion. No non-weight-bearing system was implemented. Clinical assessment, aluminum spray on the wound and perfusions check were carried out every day. No major modification of the protocol was observed during this experiment. Specimen spontaneously mobilized from the very first days. The hind legs were quite stiff during the first month. Then, a better fluidity of movement was observed until the end of the experiment. No major complication (e.g. fracture or infection) was observed. All three animals lost weight immediately postoperatively but quickly regained their pre-operative weight and over after 90 days. Similarly, for WBCC, their rate logically increased in the acute postoperative period and then gradually fell back. Fortnightly, blood sample, weighing, wound control, IV bolus injection of fluorochrome and medical imaging (Siemens Definition AS, 128 detectors) were performed. Medical imaging allowed us to qualitatively assess the bone callus evolution. Fluorochrome injections consisted of an IV bolus of tetracycline (Retardoxi 20 %®, Inovet, Arendonk, Belgium) at a dosage of 25 mg/kg [33] and calcein green solution mixture (600 mg of calcein green, C0875, Sigma-Aldrich, Saint-louis, USA, and 300 mg of sodium bicarbonate S6014, Sigma-Aldrich, Saint-Louis, USA in 20 ml of physiological liquid). The bolus dose is 10 mg/kg of calcein green. The fluorochromes were injected alternatively every fortnight until the animals were sacrificed. Each animal was euthanized after 3 months postoperatively with an IV injection of T61 (0.2 mg/kg). The allografts were then explanted and fixed with formaldehyde (4 %) for histological and immunohistochemical analysis. Explantation of the allografts was free of complications (e.g. material mobility, material breakage, infection, fracture). Dissection was straightforward, and removal of the plates and screws went smoothly.

2.5. Histological & immunohistochemical assessments

As the ossification of the allograft was one of our main concerns, explanted allografts were subjected to non-decalcified histology using laser microtomy technology (TissueSurgeon, LLS ROWIAK GmbH, Hannover, Germany). The specimens were fixed in formaldehyde (4 %) for 10 days and then embedded in spurr resin ("*Low viscosity Embedding Media Spurr's Kits*", Science Services, Munich, Germany). The histological stains used were hematoxylin/eosin (HE) as a conventional staining, Alcian blue (AB) to highlight cartilage and collagen, and Von Kossa (VK) to highlight tissue calcification.

Several immunohistochemical targets were studied. CD3 was used to assess the local inflammatory reaction by highlighting the lymphocyte populations [34]. Cellular differentiation was assessed by three different antigens: Ki67, osteocalcin (OCN). Ki67 is a universal marker of cell multiplication and proliferation [35]. OCN is a paracrine hormone secreted by osteoblasts providing evidence of their vitality and activity within the grafts. The neovascularization of the grafts was studied by targeting alpha-Smooth-Muscle Actinin (α-SMA) which highlights the smooth muscle of arterioles [36].

Unstained slides were also used to assess fluorochromes penetration through the ossification front. These molecules attach themselves to the ossification front of osteoid matrices during bone remodeling [37]. By observing the slides under the excitation wavelengths of calcein green (488 nm) and tetracycline (555 nm), we were able to highlight these ossification fronts.

All images were captured with the Microscope Axio Imager A2/ApoTome (Zeiss, Oberkochen, Germany).

2.5.1. Quantitative assessments

20 random regions of interest (ROIs) at 10× magnification were selected on each immunohistochemistry slide. Ten were taken from allograft cortex and 10 were taken from allograft medullary spaces. The quantitative evaluation of these IHC was achieved using the Q-Path® Software (v0.3.0., University of Edinburgh) by operating on a wavelength detection threshold according to each IHC signal. We were able to compare the effective IHC between native and decellularized grafts based on the percentage of positive areas that exceed the threshold in both samples.

Q-path® software was also used to measure the rate of cortical bone remodeling in our allografts. Ossification fronts visible by fluorescent microscopy were measured using a fluorescent wavelength detection threshold corresponding to the IV-injected fluorochromes. The total surface area of ossification fronts in relation to the total surface area of the allograft cortex was therefore documented, enabling another method of quantitative comparison between native and decellularized grafts.

Finally, bone remodeling activity was also quantified by counting the presence of osteoclasts on histology slides by selecting 20 ROIs at 10× magnification. All these ROIs were taken at the edge of the allograft cortex. The number of osteoclasts observed on these slides provided a final method of quantifying this bone remodeling activity.

2.5.2. Statistical analysis

All the quantitative assessments were compared using a nonparametric statistical approach of Mann-Whitney. For all tests, statistical significance threshold was set for p-values <0.05. All statistical analyses were performed using IBM SPSS Statistic software (v.27, IBM SPSS, Inc., Chicago, IL, USA). Descriptive statistics are noted as mean ± standard deviation.

3. Results

3.1. Control histology of allografts

As demonstrated in a previous study [19], histological control of decellularization confirmed the cellular clearance of the bones used to create the decellularized allografts (Fig. 3).

3.2. Imaging

No difference was qualitatively observed between groups in terms of consolidation speed on either radiography or tomography. However, a more voluminous bone callus was observed in decellularized allografts from day 75 onwards (Fig. 4).

3.3. Histology

Native histology images are showed as supplementary data.

3.3.1. H/E

We observed a dense cell population in medullary cavity of the allografts. The material in the native allografts was less dense, with signs of cellular stress and fat necrosis. In contrast, obvious angiogenesis was observed in the decellularized grafts. Low magnification acquisitions are available in supplementary data (Figs. 10a and 11a). In the cortices, the bone sections were well fused in both control and decellularized grafts. However, we observed a higher quantity of osteoclasts around the edge of the decellularized allografts, as well as larger areas of bone remodeling, deep within the allograft (Fig. 5A). This latter phenomenon was also observed in the native grafts but not in the depth of the cortex.

3.3.2. AB

Our H/E findings were confirmed by our AB staining's. However, the contrast between allogenic blue matrix and autogenic pink new bone tissue deposited by living cells was clearer (Fig. 5C). The cortical bone remodeling around vascular structures was therefore more visible. This staining also highlighted an oriented pattern in collagen fibers. Osteogenesis was observed in larger quantity in the decellularized allografts.

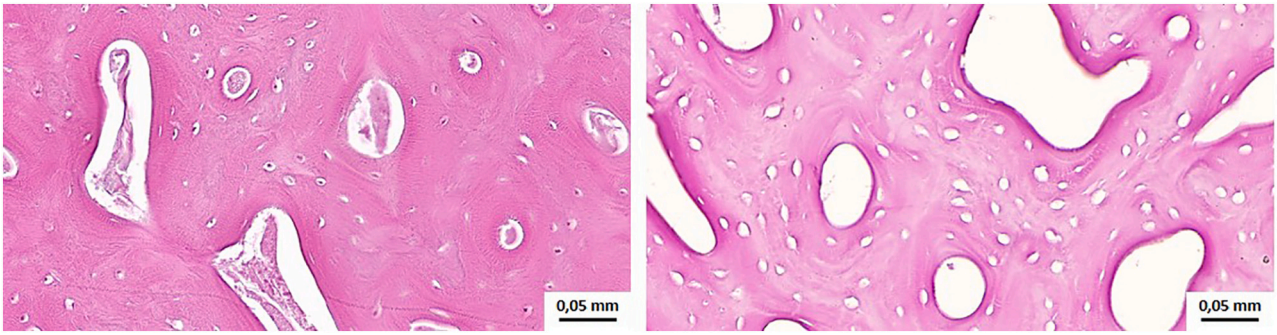

Fig. 3. Hematoxylin/eosin staining of femurs used as allografts. On the left: control allograft; osteocyte's nuclei are visible and blood material is still filling the vascular lacunae. On the right: decellularized allograft; osteoplasts and vascular lacunae are empty.

Low magnification acquisitions are available in supplementary data (Figs. 10a and 11a).

3.3.3. VK

Calcification was similar between decellularized and control grafts. However, the intramedullary surface of the cortex appeared much more active in the decellularized graft. Pre-osteogenic streaks could be seen oriented from the surface (Fig. 5D). It showed immature non-calcified tissue becoming denser closer to the surface. This phenomenon was less flagrant in the non-decellularized medullary cavity. Furthermore, a lower cell density and a border between fibrous tissue with a high cell density and a scar tissue, with a low density of cells showing lipid necrosis, was observed in this same area of native allografts (see supplementary data, Fig. 11a).

3.3.4. Osteoclasts count

Osteoclast counts on ROIs at the cortex margins of allografts demonstrated a significant difference ($p < 0.001$) between the native and decellularized allograft groups. On average, 3.86 ± 3.31 osteoclasts are visible at the edges of decellularized allografts on ROIs of 10× magnification, while an average of 1 ± 1.59 osteoclast per ROI is observed in the same histological structures of the native allografts. These observations are summarized on Fig. 5B.

3.4. Immunohistochemistry

Native IHC images are showed as supplementary data.

3.4.1. Neo-angiogenesis

3.4.1.1. α-SMA. In the medullary cavity, the development of arterial networks in both native and decellularized allografts was observed (Fig. 6A). Weak signals were observed in the cortices of decellularized allografts and in the consolidation callus (Supplementary data, Fig. 12a).

3.4.2. Cellular differentiation

3.4.2.1. Ki67. The cortices of the allografts were deprived of signal. However, the medulla of decellularized allografts appeared more positive to this marker than the medulla of native allografts (Supplementary data Fig. 13a), demonstrating greater cellular turnover and activity (Fig. 6B). This also confirmed the observations made for CD3 antigen targeting.

3.4.2.2. Osteocalcin (OCN). This IHC clearly identified the so-called creeping substitution of bone allografts. We could follow thin red positive bands at the edges of bone remodeling structures (Fig. 6C). As previously described in conventional H/E histology, we observed greater penetrance of bone remodeling in decellularized grafts. These advances in osseointegration could also be seen along the vascular lacunae of the decellularized allograft (supplementary data, Fig. 12a). At the border between the allogeneic bone and the endogenous bone, staining demonstrated the presence of active osteoblasts in the middle of the decellularized allograft. Furthermore, osteocalcin was visible along the entire length of the decellularized allograft, both on the surface and deep in the cortex. This was not observed in native grafts. At the border of the bone callus, the medullary spaces showed higher osteoblastic activity as shown in supplementary data (Fig. 13a).

3.4.3. Immunogenicity

3.4.3.1. CD3. A clear difference between the two groups was observed. The medullary cavity of the native allografts does not show any cellular activity. Immunohistochemical signal was detected on these slides. However, basal lymphocyte activity was observed in the medullary cavity of decellularized allografts and in contact with the inner surface of the cortices (Fig. 6D).

3.4.4. Quantitative assessments

Quantitative assessments using Q-Path software enabled us to measure the level and quantity of antibodies present on each non-decalcified histological slide, which can then be extrapolated to the entire allograft. In fact, this quantity is determined according to a surface ratio (positive surface in relation to the total surface of the slide). The 4 non-parametric statistical analyses, represented in Fig. 6A/B/C/D, showed that the levels of A-SMA, Ki67, OCN and CD3 were all 4 significantly higher in the decellularized allografts than in the native allografts ($p < 0.001$). Respectively studied for A-SMA, Ki67, OCN and CD3 IHC, these decellularized and native IHCs showed a mean percentage of positive area measured at: 1.35 ± 3.50 compared to 0.29 ± 0.84; 1.04 ± 2.45 compared to 0.17 ± 0.62; 1.14 ± 1.29 compared to 0.32 ± 0.44; 1.06 ± 3.52 compared to 0.01 ± 0.01.

3.5. Fluorochrome assessments

Tetracycline fluorescence (red) was lightly observed. Where we expected to see a succession of fluorescent layers alternating red and green to describe the progression of ossification, we only observed a single broad green fluorescent band superimposable between the two wavelengths.

However, counter-stains of certain IHC (CD3, Ki67) showed some artefacts in the form of orange bands into the bone tissue. These bands, fitting and superimposable to calcein fluorescent green bands, correspond to the tetracycline fixed onto the ossification front and visible in brightfield microscopy. These images are available in supplementary data (Fig. 14a).

The interest of these images lies rather in intracortical observation of

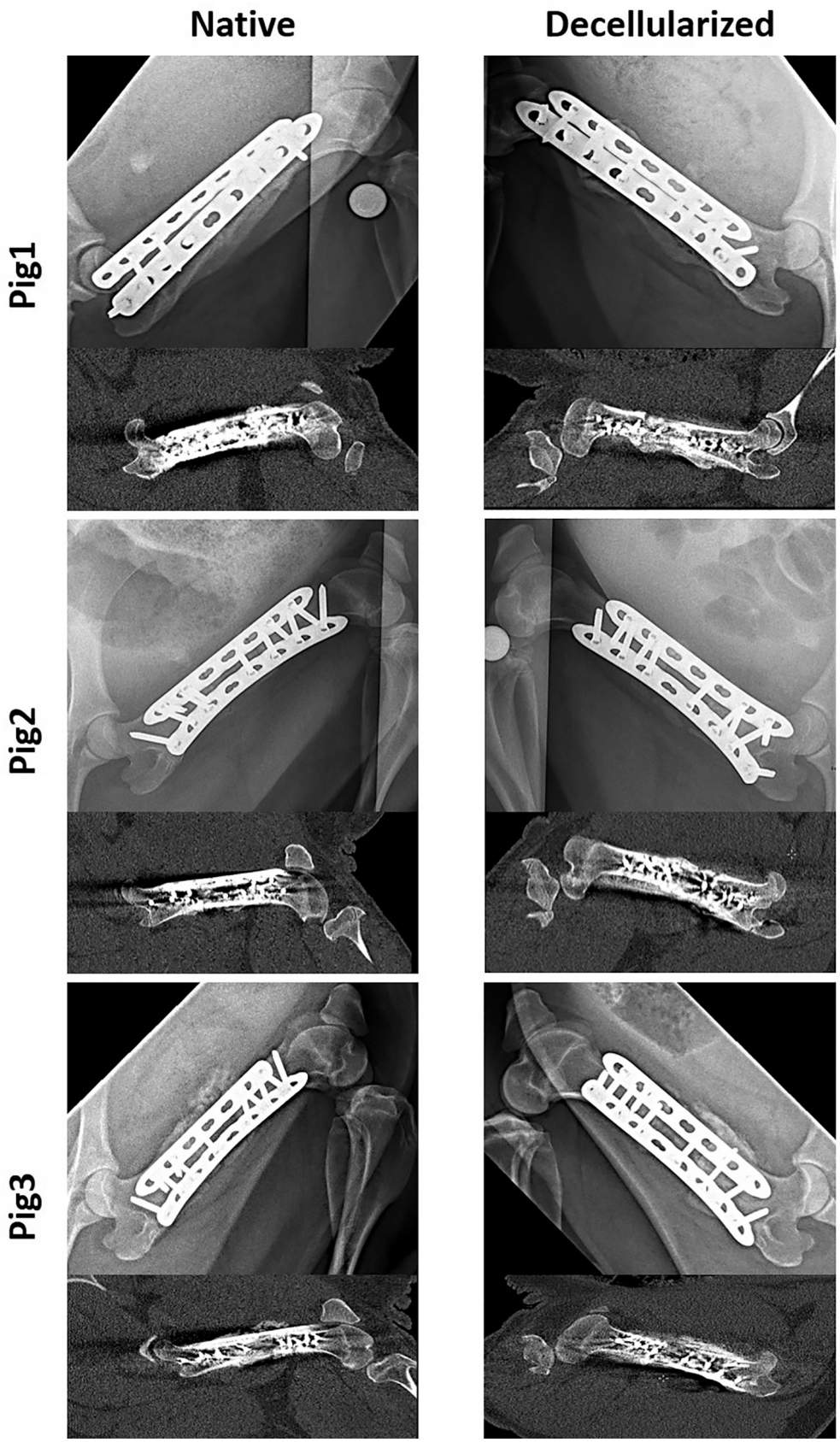

Fig. 4. Pigs clinical imaging 75 days postoperatively. X-rays (above) and tomography (below) shows profile or sagittal views of the operated femurs with native or decellularized massive bone allografts.

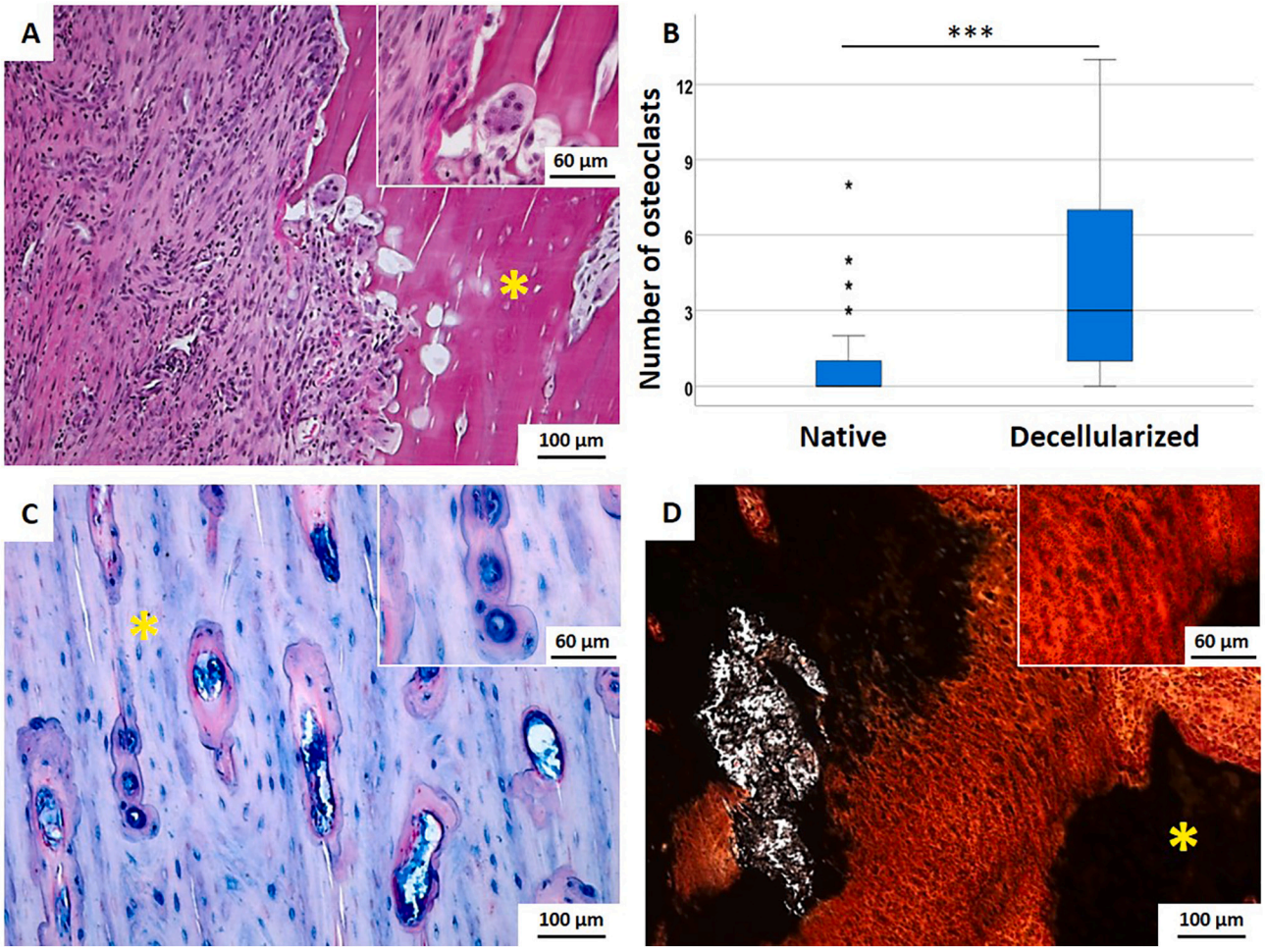

Fig. 5. Histological staining's of the explanted allografts. A: H/E staining the graft being remodeled by osteoclasts. B: The number of visible osteoclasts is significantly higher around the decellularized allograft (*** = $p < 0.001$). C: AB staining showing the decellularized matrix (yellow asterisk) being colonized by newly-formed osteons and haversian structures in darker pink (new osteocytes are visible with their lacuno-canalicular network around them). D: VK staining showing the progressive mineralization of the graft. (For interpretation of the references to colour in this figure legend, the reader is referred to the web version of this article.)

these ossification fronts. Fig. 7 shows that decellularized allografts have more active intracortical ossification fronts than native allografts and that bone remodeling reached deeper layers in the cortex. This observation demonstrates the occurrence of a greater creeping substitution in decellularized allografts, with a highly active remodeling, 3 months post-operatively. The control allografts seemed less biologically active.

Quantitative assessment of the fluorescence rate was carried out by means of a surface study. It is directly correlated with the remodeling rate of the bone graft. These green ossification fronts represent the calcein green attached to the developing osteoid matrix (Fig. 7). On average, decellularized allografts showed a percentage of positive surface area per total surface area of 7.32 ± 3.83. In comparison, native allografts exhibited an average positive surface area of 3.87 ± 3.56. Inferential statistical analysis showed a significant difference between these two groups ($p = 0.021$).

4. Discussion

This study provides a qualitative and quantitative description and proof of the superior bone integration of decellularized massive bone allografts in a large animal preclinical model. Orthotopic implantation of the two types of grafts - conventional fresh frozen versus decellularized by perfusion - allowed a detailed analysis of the different cellular actors involved in bone consolidation, integration and remodeling of those grafts. Strikingly, bone remodeling, cell colonization and angiogenesis were significantly increased in decellularized grafts. However, bone consolidation and fusion did not appear to be superior on either group from a qualitative point of view.

Two major surgeries were performed at the same time on the 3 animals in order to compare two types of allograft. Given the fact that the two grafts were implanted in the same animal on each surgery, no systemic immunogenicity studies could be carried out (i.e., immunization in blood tests). Furthermore, performing bilateral surgery on the same animal also multiplied the post-operative complications risks like infection or osteosynthesis failure. However, since the aim was to assess comparatively the integration of these grafts, we were able to compare the differential behavior of native and decellularized implants into the same general biological conditions. This choice was also made for the ethical reason of reducing the number of animals required for this experiment (3Rs rule) [38]. Additionally, this experimental model is cost-effective by reducing the number of animals required while maintaining scientific validity. It also allows for the comparison of two types of grafts under the same physiological and biomechanical conditions. Since the pattern of cellular and immune reactions is specific to each individual, being able to evaluate the biological in vivo evolution of two types of grafts under the same homeostasis—i.e., identical physiological conditions—provides valuable insights. As described above, the main limitation of this surgical model is our inability to assess the kinetics of subject immunization through repeated blood assays. Although in this experimental setup, each animal would be considered as acting as its

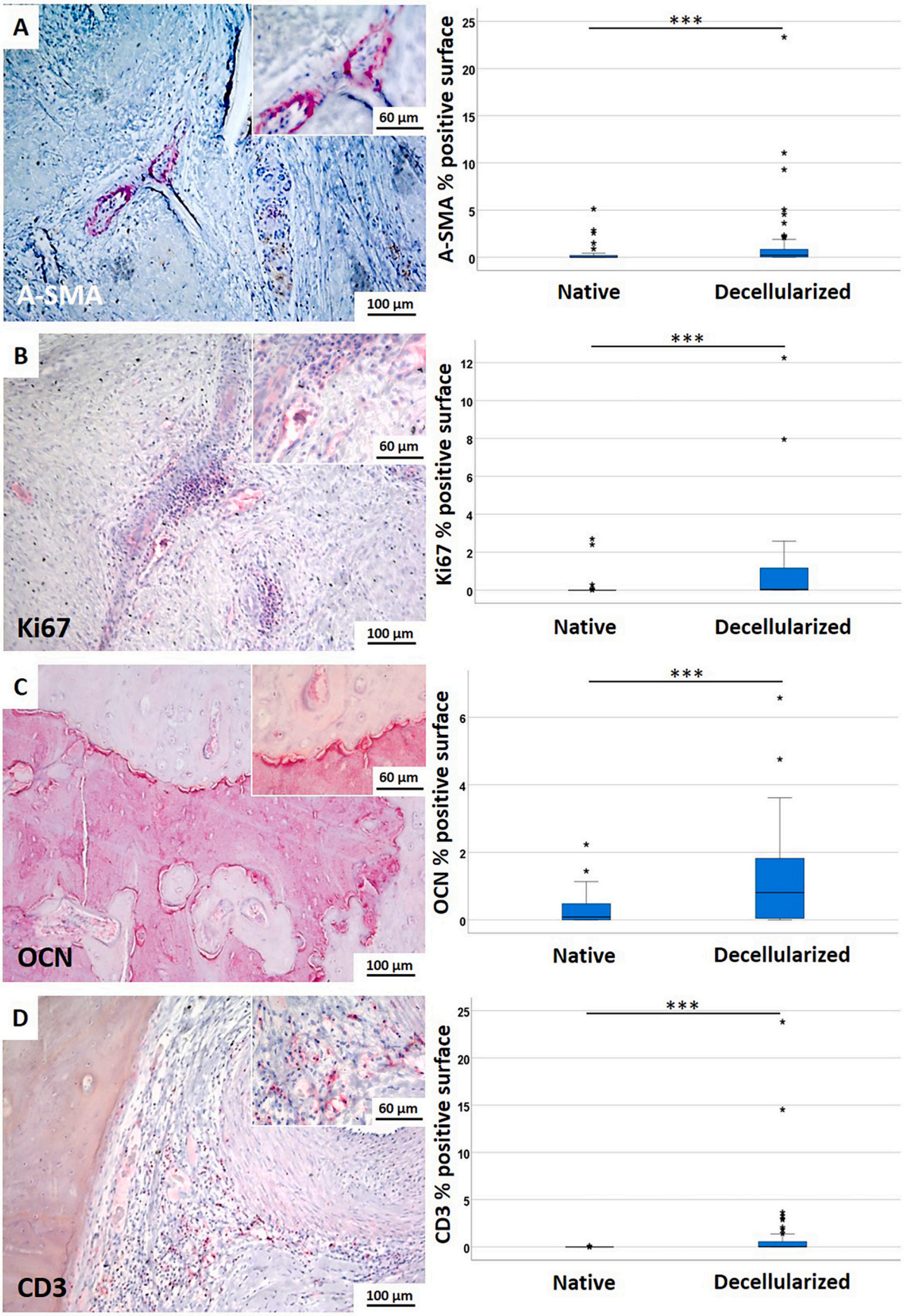

Fig. 6. Immunohistochemistry slides for α-SMA, Ki67, OCN and CD3 antibodies with their total amount quantified by Q-path software (*** = $p < 0.001$).

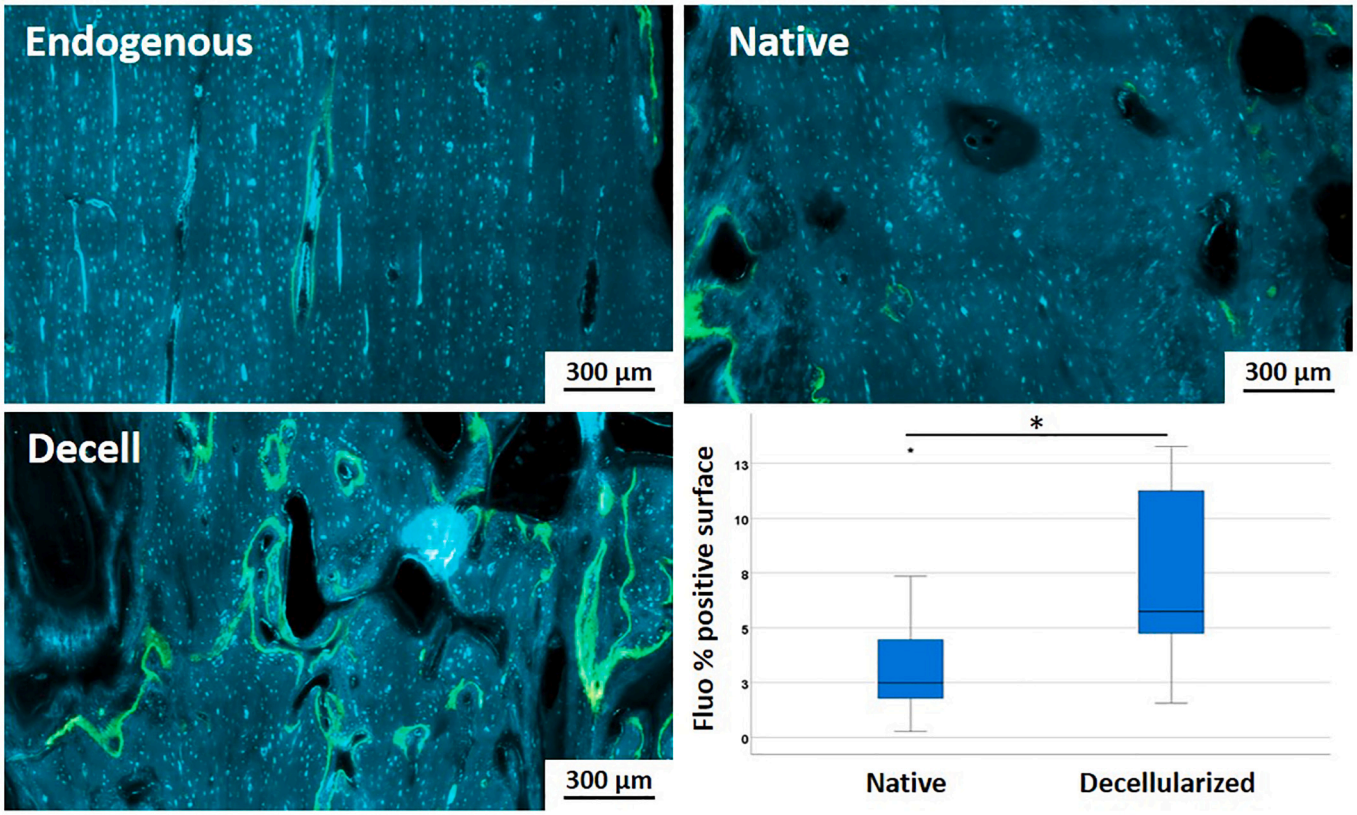

Fig. 7. Ossification front highlighted with fluorochrome injections. 488 nm wavelength excitation, fronts are visible thanks to the calcein green fixation on the active osteoid matrix present in the endogenous bone, the control allograft and the decellularized allograft. Quantification shows significant difference ($p = 0.021$) between the two types of graft. (For interpretation of the references to colour in this figure legend, the reader is referred to the web version of this article.)

own recipient-control, the conventional fresh frozen grafts were named "native" rather than "control". Indeed, the question here is what to compare with the subject of our study, which is the perfusion decellularization of massive bone allografts. We decided to compare our new type of allograft with another type of massive allograft conventionally used in humans. "Native" therefore refers to fresh-frozen allografts. The real control indeed would have been achieved with the graft harvested directly from the recipient femur in order to create the critical bone defect, and thereafter implanted back in its own donor site as a non-vascularized autograft. Our study is aiming to demonstrate the enhanced biocompatibility of the perfusion-decellularized allograft to the usual fresh frozen clinical condition. This real autologous "control" condition, which is not clinically relevant, was omitted in our experimental design.

Furthermore, as this surgical model is not currently clinically applicable, when transposing this model to humans, it will more likely involve a randomized controlled trial (RCT) comparing a group of "fresh-frozen" massive allografts to a group of "perfusion-decellularized" massive allografts regarding the patient's surgical indication, rather than using the bilateral femoral allograft approach, which remains exceedingly rare in humans, especially if the surgery occurs in a single stage, as in our preclinical animal protocol. Regarding the human translation step, the first targeted milestone we are willing to achieve is to integrate this massive bone allograft perfusion-decellularization technology into the range of techniques already offered by institutions such as tissue banks. Implementing this technology in tissue banks that can quickly set it up at low cost would be advantageous. These banks would then be able to distribute this new type of allograft, similar to how "fresh frozen" massive bone allografts are currently distributed.

Non-decalcified histology allowed a thorough graft examination without losing any information about the mineralized matrix of the calcified tissues [37]. Thereafter, conventional histological staining allowed to study the cellular event involved in the bone remodeling undergone by both types of grafts.

IHC for CD3 and Ki67 showed a higher targeting in decellularized allografts. CD3 is indicative of inflammation by targeting t-cells lymphocytes. This inflammatory process participates in bone healing by attracting crucial biological elements like growth factors, macrophages and osteoclasts or endothelial cells which stimulate cell growth, osteogenesis and angiogenesis [39]. The literature studying these phenomena has demonstrated the importance of basal inflammation to improve graft integration in other types of transplanted tissues and organs, leading to microchimerism and tolerance [40,41]. The early endogenous cellular colonization of perfusion-decellularized graft was probably favored by the strong reduction of the HLA immunogenic load previously described in the allografts [19]. This cellular invasion and viability, confirmed by Ki67 IHC, is much less observed in the native allografts, which also showed less cellular activity in the medullary cavity. In addition to the fact that the medulla of native grafts appeared biologically less active, it also exhibited signs of tissue and cell damages. Based on those observations, it seems reasonable to hypothesize that the remaining allogenic marrow material in the native allografts arises from the donor's marrow. Therefore, dead tissue that was found 3 months post-implantation is probably the result of an immune cytolytic reaction. Remnant of this allogeneic material so prevent the cellular invasion process that is essential for the consolidation and angiogenesis in bone tissue healing. Conversely, since the decellularized allograft is completely cleansed of all this allogenic material both in the medulla and in the cortex, its endogenous colonization occurs faster and results in a higher bone remodeling initiated by osteoclastic invasion of the mineralized matrix, thereafter followed by new autologous bone apposition. These medullar events were also emphasized by mineral VK staining, leading to same

conclusions. As a matter of facts, it seems obvious that the endogenous cell colonization is more efficient in decellularized allografts because both medullar spaces and bone cortices have been completely depleted of adverse allogenic remnants of the donor.

This hypothesis is also reinforced by the osteocalcin marking, which was more predominant in the decellularized allografts than in the native ones. This observation shows how the creeping substitution is more widely and more deeply spread in the decellularized massive bone allografts, bringing an additional proof that a decellularized allograft quickly behaves more likely as a non-living matrix rather than a fresh frozen allograft [42]. The fact that allogeneic tissues are removed allows an earlier and deeper bone colonization and remodeling by the visible phenomenon on H/E and AB staining's, improving the bio-integration of these grafts [13].

IHCs targeting α-SMA also showed a greater amount of arterial vascular tissue in the decellularized allografts. This is also a strong argument favoring the hypothesis that one type of graft has biological characteristics more prone to cellular integration and colonization. As neoangiogenesis is crucial for any stage of tissue healing and for any type of tissue, our results demonstrate that perfusion-decellularized bone grafts are more viable and undergo better integration than conventional native grafts.

Our study however has multiple limitations. The first one is due to the limited duration of the experiment. An important information that could have been verified if the experiment had lasted longer, was that the medullary cavity seemed to be progressively occluded and obliterated by the growth of the endosteal callus in the native allografts. It is well-known that the medullary canal must be vascularized and biologically active if we want to promote bone healing and to avoid bone necrosis [43,44]. Evidence of progressive medullary canal occlusion (supplementary data) was visible in many sections. This endosteal callus is a good sign of bone healing, but if it completely closes the medullary space, it would be an additional argument for encouraging the deep cleaning of the bone graft and its medullary cavity in order to accelerate complete colonization of this tissue before the canal is obliterated by the endosteal callus. Our study protocol stopped the follow-up at 3 months. The biological differences mentioned here could have been better observed with a longer follow-up. In addition, the mechanical constraints would have had much more impact, because the animals mobilized better throughout the weeks. Furthermore, with a longer delay before sacrifice, we could also have observed and studied the occurrence of chronic complications such as non-union or stress fracture [11,45].

The interdependence of the two lower limbs of the pig is another limitation. However, this bias is relatively small compared to the benefit of evaluating these allografts in the same individual, as described above. Furthermore, since no non-weight bearing method was implemented in our protocol, each individual was able to apply complete and direct weight bearing on the limbs upon wakening from anesthesia. As the surgeries were precisely identical on both sides, the symmetry of the procedure and the correct dosage of analgesics minimized the appearance of asymmetry in gait or weight-bearing between the two femurs. In comparison, a single-side surgery will create a significant asymmetry in the animal gait. Furthermore, we have recently shown that applying a non-physiologic load on our perfusion-decellularized can compromise its mechanical resilience [46]. Consequently, both allografts were subjected to the same mechanical stresses from the moment they woke up.

Unfortunately, some histological stains and immunohistochemical markers were not sufficiently specific to be used in this study. Stains that would have been valuable for confirming our results, such as TRAP for “Tartrate-Resistant Acid Phosphatase” (specific to osteoclasts [47]), RUNX2 (a nuclear promoter for chondrogenic differentiation [48]), and CD31 (an endothelial cell marker [49]), did not yield conclusive or exploitable results. This is likely due to the relatively limited use of the porcine species in fundamental animal experimentation, resulting in a scarcity of species-specific antibodies on the market, or antibodies whose efficacy is largely anecdotal and unpublished.

As a pilot study, the number of studied specimens is still small. All pilot studies suffer from this limitation, which makes it risky to generalize the results. Now that these experiments have yielded conclusive results, it is essential to attempt to carry out studies with larger cohorts through efficient power analysis. Moreover, to complete this research, three studies are currently underway in our laboratories: a biomechanical study comparing allografts before and after implantation, and two studies using the same surgical model and assessing different types of orthopedic osteosynthesis or bone substitute. The biomechanical study will continue to characterize this new type of perfusion-decellularized massive bone allograft ex vivo. Additionally, the study will be enhanced by advanced imaging techniques, such as micro-CT, to assess the architecture of these grafts.

The present study demonstrated the determining role of a thorough decellularization and cleaning of the allograft. The medullary cavity and cortical spaces must be as free as possible, to leave space for recolonization and graft viability. The medulla has to be emptied of any immunogenic cellular debris. However, after 3 months, this experience shows that the biological results may still be improved.

After harvesting and decellularization, three more steps may be implemented to further improve this model (Fig. 8). The third step, currently ongoing in our laboratories, involves bone recellularization by perfusion of stem cells harvested from the future recipient, prior to implantation (Fig. 8, step 3). As part of the path to bring life back to the allografts, restoring their biologically active cellular content is a major step towards better integration. The first aim is not to be able to implant directly a full living bone, but to provide an additional boost of cells, paracrine effects and growth factors to the graft's ability to osseointegrate. As demonstrated in our previous study indeed, perfusion-decellularized bone grafts retain their vascular channels network by which a wide spread of stem cells in the decellularized bone matrix will be possible [50], by slow infusion through the preserved arterial pedicle. This step should ideally be performed before reendothelialization in order to allow stem cells to enter bone lacunae and to line apposition surfaces. The fourth step is aiming to exploit the nutrient artery of our bone grafts in the best possible way (Fig. 8, step 4). The principle being to treat bone tissue as an organ at the time of implantation. This could be achieved by using its preserved vascular access in order to perform an arterial anastomosis, so obtaining a vascularized bone graft. This necessitate however, before implantation, the full restoration of an endovascular coating of the preserved vascular channels in order to avoid a massive clotting of the capillary bed and fast arterial thrombosis. For this purpose, an endothelial recellularization protocol is currently being studied in our laboratories. At the present however, similar attempts of advanced organ fabrication by the perfusion-decellularization strategy have emphasized several technical limitations to overcome this difficulty and to unlock the critical step in vascularized composite tissue engineering [16,17]. The final and ultimate achievement of our model, combining step 3 and 4 should then be able to create a fully allocompatible vascularized bone graft in which the remaining contribution of the donor should be restricted to the non-immunogenic mineralized bone matrix (Fig. 8, step 5). The so obtained “living” bone grafting partially recellularized and fully reendothelialized in vitro, should then be revascularized in vivo by performing vascular anastomosis on the arterial and venous pedicle previously used as an access for growth factor and osteogenic stem cells infusion and full endothelial coating of the decellularized vascular network. This anastomosis strategy has already been proven efficient in various tissue engineering models [16,17,51]. As in step 3, the bone cellular content of the graft has not to be entirely restored. The recipient will become its own bioreactor after implantation through the natural process of Haversian bone remodeling, which should be spatially enhanced in the whole graft volume by revascularization and thus by the restoration of the intrinsic bone microvascular supply required for bone consolidation. The three combined approaches could thus bring us as close as possible to a living

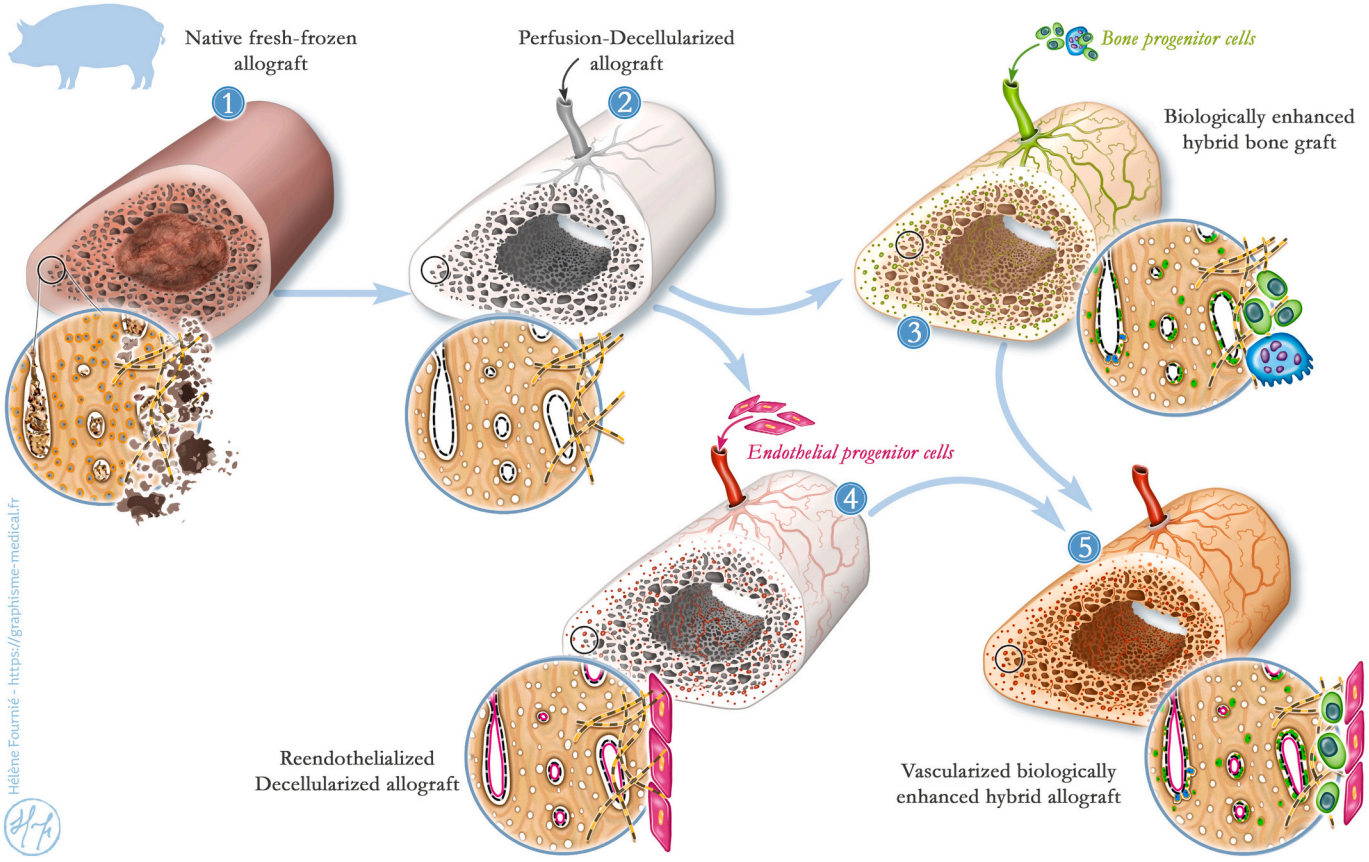

Fig. 8. Perspectives and research plan of the perfusion-decellularized bone model. Step 1: harvesting step, as in human clinics as massive bone allografts are used-without any treatment, filled with immunogenic cellular debris. Step 2: preservation of the nutrient artery, perfusion-decellularization protocol and acquisition of a non-immunogenic massive allograft. Step 3: Recellularization of the allograft with stem cells slow infusion through the vascular network. Step 4: Reendothelialization of the allograft with endothelial stem cells in order to fully coat the preserved basal membrane. Step 5: merging both step 3 and 4.

massive allocompatible bone graft, with its own vascularization and cellular vitality.

5. Conclusion

This preclinical pilot study demonstrates the biological superiority of intercalary massive bone allografts decellularized by perfusion compared to conventional fresh frozen massive bone allografts. It is an interesting progression of our laboratories work and expertise and it offers a reliable model for further experiments and investigations aiming to create allocompatible bone graft step by step. This latter conceptual endpoint of our research will however require major concomitant advances in the perfusion-decellularization protocol technology and in tissue engineering methods before becoming fully translatable as an innovative surgical tool to human clinical purpose.

Supplementary data to this article can be found online at https://doi.org/10.1016/j.bone.2024.117213.

Funding statement

The authors declare that this work has been achieved thanks to the specific funding of the *Fondation Christian Delloye*. Robin Evrard, Julie Manon and Louis Maistriaux are Research Aspirants of the FNRS (Fonds National de la Recherche Scientifique, Applications ID 40010491, ID 40004991 and ID 40000380 respectively, Belgium). Tom Darius is also funded by the FNRS as Researcher (ID: FRNS-CDR J.00.36.21).

CRediT authorship contribution statement

Robin Evrard: Writing – original draft, Validation, Methodology, Investigation, Formal analysis, Data curation, Conceptualization. **Julie Manon:** Writing – original draft, Investigation, Formal analysis, Data curation. **Louis Maistriaux:** Writing – original draft, Investigation, Formal analysis. **Lies Fievé:** Writing – original draft, Methodology, Formal analysis, Data curation. **Tom Darius:** Writing – review & editing, Validation, Methodology, Conceptualization. **Olivier Cornu:** Writing – review & editing, Supervision, Resources, Project administration, Methodology, Conceptualization. **Benoit Lengelé:** Writing – review & editing, Visualization, Supervision, Project administration, Methodology, Conceptualization. **Thomas Schubert:** Writing – review & editing, Visualization, Validation, Supervision, Resources, Methodology, Funding acquisition, Conceptualization.

Declaration of generative AI and AI-assisted technologies in the writing process

During the preparation of this work the author(s) used ChatGPT and DeepL in order to enhance the scientific English grammar and spelling of this work. After using this tool/service, the author(s) reviewed and edited the content as needed and take(s) full responsibility for the content of the publication.

Declaration of competing interest

None.

Data availability

Data will be made available on request.

References

[1] M. Gage, F. Liporace, K. Egol, T. McLaurin, Management of bone defects in orthopedic trauma, Bull. Hosp. Jt Dis. 2018 (76) (2013) 4–8.
[2] C. Zou, Z. Zhao, T. Lin, Y. Huang, X. Xie, J. Yin, et al., Long-term outcomes of limb salvage treatment with custom-made extendible endoprosthesis for bone sarcoma around the knee in children, J. Orthop. Surg. 15 (2020) 14, https://doi.org/10.1186/s13018-019-1534-x.
[3] T. Bormann, S. Jäger, J.P. Kretzer, L. Nebel, L. Clarius, G. Omlor, et al., Retrieval analysis of modern knee tumor megaendoprosthesis shows considerable volumetric metal wear generated at the rotating hinge, Mater Basel Switz 13 (2020) 1519, https://doi.org/10.3390/ma13071519.
[4] A.H. Schmidt, Autologous bone graft: is it still the gold standard? Injury 52 (Suppl. 2) (2021) S18–S22, https://doi.org/10.1016/j.injury.2021.01.043.
[5] P. Baldwin, D.J. Li, D.A. Auston, H.S. Mir, R.S. Yoon, K.J. Koval, Autograft, allograft, and bone graft substitutes: clinical evidence and indications for use in the setting of orthopaedic trauma surgery, J. Orthop. Trauma 33 (2019) 203–213, https://doi.org/10.1097/BOT.0000000000001420.
[6] N. Shibuya, D.C. Jupiter, Bone graft substitute: allograft and xenograft, Clin. Podiatr. Med. Surg. 32 (2015) 21–34, https://doi.org/10.1016/j.cpm.2014.09.011.
[7] W.W. Tomford, Bone allografts: past, present and future, Cell Tissue Bank. 1 (2000) 105–109, https://doi.org/10.1023/A:1010158731885.
[8] A.C. Masquelet, T. Begue, The concept of induced membrane for reconstruction of long bone defects, Orthop Clin North Am 41 (2010) 27–37, table of contents, https://doi.org/10.1016/j.ocl.2009.07.011.
[9] C. Benulic, G. Canton, I. Gril, L. Murena, A. Kristan, Management of acute bone loss following high grade open tibia fractures. Review of evidence on distraction osteogenesis and induced membrane techniques, Acta Bio Medica Atenei Parm 91 (2020) e2020012, https://doi.org/10.23750/abm.v91i14-S.10890.
[10] W.W. Tomford, H.J. Mankin, Bone banking., Update on methods and materials, Orthop. Clin. North Am. 30 (1999) 565–570, https://doi.org/10.1016/s0030-5898(05)70109-7.
[11] C. Delloye, M. van Cauter, D. Dufrane, B.G. Francq, P.-L. Docquier, O. Cornu, Local complications of massive bone allografts: an appraisal of their prevalence in 128 patients, Acta Orthop. Belg. 80 (2014) 196–204.
[12] Z. Matejovsky, Z. Matejovsky, I. Kofranek, Massive allografts in tumour surgery, Int. Orthop. 30 (2006) 478–483, https://doi.org/10.1007/s00264-006-0223-7.
[13] C. Delloye, How to improve the incorporation of massive allografts? Chir. Organi Mov. 88 (2003) 335–343.
[14] F. Blaudez, S. Ivanovski, S. Hamlet, C. Vaquette, An overview of decellularisation techniques of native tissues and tissue engineered products for bone, ligament and tendon regeneration, Methods San Diego Calif 171 (2020) 28–40, https://doi.org/10.1016/j.ymeth.2019.08.002.
[15] P.M. Crapo, T.W. Gilbert, S.F. Badylak, An overview of tissue and whole organ decellularization processes, Biomaterials 32 (2011) 3233–3243, https://doi.org/10.1016/j.biomaterials.2011.01.057.
[16] H.C. Ott, T.S. Matthiesen, S.-K. Goh, L.D. Black, S.M. Kren, T.I. Netoff, et al., Perfusion-decellularized matrix: using nature's platform to engineer a bioartificial heart, Nat. Med. 14 (2008) 213–221, https://doi.org/10.1038/nm1684.
[17] J. Duisit, H. Amiel, T. Wüthrich, A. Taddeo, A. Dedriche, V. Destoop, et al., Perfusion-decellularization of human ear grafts enables ECM-based scaffolds for auricular vascularized composite tissue engineering, Acta Biomater. 73 (2018) 339–354, https://doi.org/10.1016/j.actbio.2018.04.009.
[18] N. Poornejad, N. Momtahan, A.S.M. Salehi, D. Scott, C. Fronk, B. Roeder, et al., Efficient decellularization of whole porcine kidneys improves reseeded cell behavior, Biomed. Mater. 11 (2016) 025003, https://doi.org/10.1088/1748-6041/11/2/025003.
[19] R. Evrard, J. Manon, L. Maistriaux, C. Rafferty, L. Fieve, U. Heller, et al., Decellularization of massive bone allografts by perfusion: a new protocol for tissue engineering, Tissue Eng. Part A (2023), https://doi.org/10.1089/ten.TEA.2023.0182.
[20] P. Cravedi, S. Farouk, A. Angeletti, L. Edgar, R. Tamburrini, J. Duisit, et al., Regenerative immunology: the immunological reaction to biomaterials, Transpl Int Off J Eur Soc Organ Transplant 30 (2017) 1199–1208, https://doi.org/10.1111/tri.13068.
[21] M. van Steenberghe, T. Schubert, S. Gerelli, C. Bouzin, Y. Guiot, D. Xhema, et al., Porcine pulmonary valve decellularization with NaOH-based vs detergent process: preliminary in vitro and in vivo assessments, J. Cardiothorac. Surg. 13 (2018) 34, https://doi.org/10.1186/s13019-018-0720-y.
[22] T.H. Petersen, E.A. Calle, L. Zhao, E.J. Lee, L. Gui, M.B. Raredon, et al., Tissue-engineered lungs for in vivo implantation, Science 329 (2010) 538–541, https://doi.org/10.1126/science.1189345.
[23] T.J. Keane, I.T. Swinehart, S.F. Badylak, Methods of tissue decellularization used for preparation of biologic scaffolds and in vivo relevance, Methods San Diego Calif 84 (2015) 25–34, https://doi.org/10.1016/j.ymeth.2015.03.005.
[24] U. Heller, R. Evrard, B. Lengelé, T. Schubert, N. Kadlub, J. Boisson, Decellularized vascularized bone grafts as therapeutic solution for bone reconstruction: a mechanical evaluation, PLoS One 18 (2023) e0280193, https://doi.org/10.1371/journal.pone.0280193.
[25] G. Rougier, L. Maistriaux, L. Fievé, D. Xhema, R. Evrard, J. Manon, et al., Decellularized vascularized bone grafts: a preliminary in vitro porcine model for bioengineered transplantable bone shafts, Front. Bioeng. Biotechnol. 10 (2022) 1003861, https://doi.org/10.3389/fbioe.2022.1003861.
[26] J. Manon, R. Evrard, L. Fievé, C. Bouzin, D. Magnin, D. Xhema, et al., A new osteogenic membrane to enhance Bone healing: at the crossroads between the periosteum, the induced membrane, and the diamond concept, Bioengineering 10 (2023) 143, https://doi.org/10.3390/bioengineering10020143.
[27] M. Cummaudo, A. Cappella, F. Giacomini, C. Raffone, N. Màrquez-Grant, C. Cattaneo, Histomorphometric analysis of osteocyte lacunae in human and pig: exploring its potential for species discrimination, Int. J. Legal Med. 133 (2019) 711–718, https://doi.org/10.1007/s00414-018-01989-9.
[28] K. Pawlowsky, L. Ernst, J. Steitz, T. Stopinski, B. Kögel, A. Henger, et al., The Aachen Minipig: phenotype, genotype, hematological and biochemical characterization, and comparison to the Göttingen Minipig, Eur. Surg. Res. 58 (2017) 193–203, https://doi.org/10.1159/000471483.
[29] M. van Steenberghe, T. Schubert, C. Bouzin, C. Caravaggio, Y. Guiot, D. Xhema, et al., Enhanced vascular biocompatibility and remodeling of decellularized and secured xenogeneic/allogeneic matrices in a porcine model, Eur Surg Res Eur Chir Forsch Rech Chir Eur 59 (2018) 58–71, https://doi.org/10.1159/000487591.
[30] T. Schubert, S. Lafont, G. Beaurin, G. Grisay, C. Behets, P. Gianello, et al., Critical size bone defect reconstruction by an autologous 3D osteogenic-like tissue derived from differentiated adipose MSCs, Biomaterials 34 (2013) 4428–4438, https://doi.org/10.1016/j.biomaterials.2013.02.053.
[31] D. Kotsougiani, C.A. Hundepool, L.F. Bulstra, P.F. Friedrich, A.Y. Shin, A.T. Bishop, Bone vascularized composite allotransplantation model in swine tibial defect: evaluation of surgical angiogenesis and transplant viability, Microsurgery 39 (2019) 160–166, https://doi.org/10.1002/micr.30310.
[32] A. Nauth, E. Schemitsch, B. Norris, Z. Nollin, J.T. Watson, Critical-size bone defects: is there a consensus for diagnosis and treatment? J. Orthop. Trauma 32 (Suppl. 1) (2018) S7–11, https://doi.org/10.1097/BOT.0000000000001115.
[33] O. Ristow, D. Nehrbass, S. Zeiter, D. Arens, J. Moratin, C. Pautke, et al., Differences between auto-fluorescence and tetracycline-fluorescence in medication-related osteonecrosis of the jaw-a preclinical proof of concept study in the mini-pig, Clin. Oral Investig. 24 (2020) 4625–4637, https://doi.org/10.1007/s00784-020-03332-2.
[34] P.A. Kirkham, H. Takamatsu, H. Yang, R.M. Parkhouse, Porcine CD3 epsilon: its characterization, expression and involvement in activation of porcine T lymphocytes, Immunology 87 (1996) 616–623.
[35] MKI67 marker of proliferation Ki-67 [Sus scrofa (pig)] - Gene - NCBI n.d. https://www.ncbi.nlm.nih.gov/gene/102164100 (accessed July 26, 2023).
[36] S. Cherng, J. Young, H. Ma, Alpha-smooth muscle actin (α-SMA), J. Am. Sci. (2008) 4.
[37] C.-C. Hung, E. Fu, H.-C. Chiu, H.-C. Liang, Bone formation following sinus grafting with an alloplastic biphasic calcium phosphate in Lanyu Taiwanese mini-pigs, J. Periodontol. 91 (2020) 93–101, https://doi.org/10.1002/JPER.17-0748.
[38] R.G.W. Kirk, Recovering the principles of humane experimental technique, Sci. Technol. Hum. Values 43 (2018) 622–648, https://doi.org/10.1177/0162243917726579.
[39] T.J. Koh, L.A. DiPietro, Inflammation and wound healing: the role of the macrophage, Expert Rev. Mol. Med. 13 (2011) e23, https://doi.org/10.1017/S1462399411001943.
[40] T.E. Starzl, Chimerism and tolerance in transplantation, Proc. Natl. Acad. Sci. USA 101 (Suppl. 2) (2004) 14607–14614, https://doi.org/10.1073/pnas.0404829101.
[41] T.E. Starzl, A.S. Rao, M. Trucco, P. Fontes, J.J. Fung, A.J. Demetris, Explanation for loss of the HLA matching effect, Transplant. Proc. 27 (1995) 57–60.
[42] H. Huang, C. Jiang, Z. Feng, X. Jiang, Comparing the process of creeping substitution between allograft bone and local bone grafting in lumbar interbody fusion, Eur Spine J Off Publ Eur Spine Soc Eur Spinal Deform Soc Eur Sect Cerv Spine Res Soc 23 (2014) 2068–2074, https://doi.org/10.1007/s00586-014-3388-6.
[43] R.G. Burwell, The function of bone marrow in the incorporation of a bone graft, Clin. Orthop. (1985) 125–141.
[44] Q. Zhao, X. Liu, C. Yu, Y. Xiao, Macrophages and bone marrow-derived mesenchymal stem cells work in concert to promote fracture healing: a brief review, DNA Cell Biol. 41 (2022) 276–284, https://doi.org/10.1089/dna.2021.0869.
[45] P.H.J. Bullens, N.M. Minderhoud, M.C. de Waal Malefijt, R.P.H. Veth, P. Buma, H. W.B. Schreuder, Survival of massive allografts in segmental oncological bone defect reconstructions, Int. Orthop. 33 (2009) 757–760, https://doi.org/10.1007/s00264-008-0700-2.
[46] R. Evrard, M. Feyens, J. Manon, B. Lengelé, O. Cartiaux, T. Schubert, Impact of NaOH based perfusion-decellularization protocol on mechanical resistance of structural bone allografts, Connect. Tissue Res. (2024) 1–14, https://doi.org/10.1080/03008207.2024.2356586.
[47] S.L. Teitelbaum, Bone resorption by osteoclasts, Science 289 (2000) 1504–1508, https://doi.org/10.1126/science.289.5484.1504.
[48] RUNX2 RUNX family transcription factor 2 [Sus scrofa (pig)] - Gene - NCBI n.d. https://www.ncbi.nlm.nih.gov/gene/100737965 (accessed July 26, 2023).

[49] F.M. Marelli-Berg, M. Clement, C. Mauro, G. Caligiuri, An immunologist's guide to CD31 function in T-cells, J. Cell Sci. 126 (2013) 2343–2352, https://doi.org/10.1242/jcs.124099.

[50] R. Evrard, J. Manon, C. Rafferty, L. Fieve, O. Cornu, T. Kirchgesner, et al., Vascular study of decellularized porcine long bones: characterization of a tissue engineering model, Bone (2024) 182, https://doi.org/10.1016/j.bone.2024.117073.

[51] P. Akhyari, H. Kamiya, P. Gwanmesia, H. Aubin, R. Tschierschke, S. Hoffmann, et al., In vivo functional performance and structural maturation of decellularised allogenic aortic valves in the subcoronary position, Eur J Cardio-Thorac Surg Off J Eur Assoc Cardio-Thorac Surg 38 (2010) 539–546, https://doi.org/10.1016/j.ejcts.2010.03.024.